Journal of Sound and Vibration 425 (2018) 1–20

Contents lists available at ScienceDirect

Journal of Sound and Vibration

journal homepage: www.elsevier.com/locate/jsvi

Sound absorption of a porous material with a perforated facing at high sound pressure levels

Feng Peng

Key Laboratory of Noise and Vibration Research, Institute of Acoustics, Chinese Academy of Sciences, Beijing 100190, China

ARTICLE INFO

Article history:
Received 8 November 2017
Received in revised form 4 February 2018
Accepted 26 March 2018
Available online 7 April 2018

Keywords:
Sound absorption
Porous material
Perforated facing
High sound pressure level

ABSTRACT

A semi-empirical model is proposed to predict the sound absorption of an acoustical unit consisting of a rigid-porous material layer with a perforated facing under the normal incidence at high sound pressure levels (SPLs) of pure tones. The nonlinearity of the perforated facing and the porous material, and the interference between them are considered in the model. The sound absorptive performance of the acoustical unit is tested at different incident SPLs and in three typical configurations: 1) when the perforated panel (PP) directly contacts with the porous layer, 2) when the PP is separated from the porous layer by an air gap and 3) when an air cavity is set between the porous material and the hard backing wall. The test results agree well with the corresponding theoretical predictions. Moreover, the results show that the interference effect is correlated to the width of the air gap between the PP and the porous layer, which alters not only the linear acoustic impedance but also the nonlinear acoustic impedance of the unit and hence its sound absorptive properties.

1. Introduction

Traditional perforated panel resonator has received a lot of attention in the control of noise with high sound intensity in the early stage of development, mainly because it has simple configuration and is not readily to be polluted. It has been used in a number of environments with high SPL, such as the acoustic liner of aero-engine. In recent years, researchers [1] also considered the application of micro-perforated panel in the interior of launcher fairings to reduce the internal acoustic load with high intensity. Further studies have been published on the acoustic characteristics and sound absorptive mechanism of the PP and the acoustic liner consisting of a PP and honeycombs under high SPL [2–9]. These results indicate that the sound absorptive properties of a PP depend on the incident SPL, i.e. exhibiting nonlinear sound absorption characteristics. Different from viscous dissipation under low SPL, the sound absorption mechanism under high-amplitude acoustic excitation is mainly dissipation in the jet formed at the exit and via the vortex shedding at the sharp edge of orifice [2,4,6,8,9]. It should be pointed out that the effective band of high sound absorption of a perforated plate is normally limited in the lower frequency range and high sound absorption is difficult to realize in the middle-to-high frequency range, while many intense noise sources in practice contain not only pure tones of middle-to-high frequencies, but also broadband components, such as the noise at the inlet of aircraft engine [10]. Accordingly, this study mainly focuses on the sound absorption of an absorber in the middle-to-high frequency range.

E-mail address: pengfeng@mail.ioa.ac.cn.

https://doi.org/10.1016/j.jsv.2018.03.028
0022-460X/

Excellent performance such as wide band and high sound absorption in the middle-to-high frequency range can be readily realized by proper design and selection of porous material, which has been widely used in the field of noise control. The linear acoustic model of porous materials is relatively sophisticated, and a few studies have been conducted on the nonlinear acoustic characteristics of porous materials [11–22]. Among these studies, Wilson et al. [14] proposed a corrected form of the equivalent complex density of material by using the static flow resistance relation of Forchheimer's law [23], and pointed out that the Forchheimer-type nonlinearity might be the dominant type of nonlinearity for the propagation of high-amplitude acoustic waves in porous media. McIntosh and Lambert [15,16] studied the effects of viscosity and thermal conduction within porous material under high SPL and pointed out that the nonlinear effect of viscosity is significant, while the nonlinear thermal effect is not. Aurégan and Pachebat [17] measured the flow resistivity elaborately and found two types of seepage velocity regions; after comparing an equivalent fluid model with acoustic measurements for high-level sound propagation in rigidly framed porous media, they pointed out that the increase in flow resistivity describes the main nonlinear effect. Umnova and Attenborough et al. proposed models to predict reflection coefficient of single-layer [18] and multi-layer [19] porous material backed by hard wall under high SPL; in their models, the static flow resistivity in equivalent fluid model was directly replaced with the resistivity which is linear with airflow velocity, i.e. Forchheimer's correction. Peng et al. [20,21] used the linearization method and finite difference method to solve the particle velocity inside the porous layer with rigid frame and finite thickness under high SPL and further predicted the nonlinear sound absorptive properties of the layer. Zhang et al. [22] used the 4th-order Runge-Kutta method to solve the Ricatti equation for the acoustic admittance of porous material under high SPL and then predicted the sound absorption.

In many practical applications, a porous layer usually need to be covered by a perforated facing (i.e. a hard perforated panel) to protect the material and improve the surface stiffness of the structure. There have been a number of studies on the characteristics of this type of sound absorptive structure under linear conditions [24–29], but the sound absorption properties under high SPL are less studied because both the PP and the porous material display nonlinear characteristics and it is more complicated to construct a theoretical model. Tayong et al. [30] predicted the sound absorption of a porous layer covered with a micro-perforated panel under high sound excitation using an approach based on the equivalent fluid method. In their studies, the transfer matrix method was adopted for the coupling between the micro-perforated panel and the porous layer, and the flow resistivity of each layer was corrected with the Forchheimer's law. However, it should be pointed out that when the acoustic nonlinearity inside a porous material is considered, its characteristic impedance and propagation constant are no longer irrelevant to the local particle velocity; moreover, the amplitude of the particle velocity in a porous material with finite thickness varies in the direction of propagation. Hence the transmission line method or transfer matrix method used in linear problems cannot be applied under the nonlinear condition [14,19]. Although the results predicted by Tayong agreed with the experimental results, the details of dealing with the nonlinearity of porous material using the transfer matrix method were not described; meanwhile, the perforation ratio of the micro-perforated panel in their experiment is very low (less than 2%), so the nonlinearity of the PP may be dominant, and the nonlinearity of porous layer could not be significantly reflected in the predicted results. In addition, Tayong only put the nonlinear static flow resistivity of the PP and the porous layer into respective equivalent fluid models, without considering the interference effect, i.e. the jet that may be formed at the end of the perforations will interfere with the porous layer, thus affecting the nonlinear absorption characteristics of the whole unit.

This study investigates the sound absorption characteristics of an acoustical unit consisting of a porous material with rigid frame covered by a perforated facing under high sound pressure excitation, with the aim of constructing a simple model that can predict the nonlinear absorptive properties of such an acoustical unit. The nonlinearity of the PP and the porous material, and the nonlinear effect brought by the interference between them are considered in the model. The model is described in Section 2, and the experiments conducted to validate the model are introduced in Section 3, including the related experimental setups and the comparison of experimental results with theoretical predictions. The influences of the air gap between the porous layer and the PP are discussed. Finally, conclusions are drawn in Section 4.

2. Model of the nonlinear absorption of the acoustical unit

The sound absorptive unit consisting of a porous layer covered with a PP is illustrated in Fig. 1. At the incidence of sound with high SPL, the characteristic impedance and propagation constant of the porous material may not be independent on the acoustic particle velocity because of the nonlinear effect, so neither the impedance transmission line method nor the transfer matrix method is applicable. Meanwhile, when the SPL is high enough, previous study [2] showed that the impedance of a PP may be altered by the nonlinear effect associated with jet and vortex shedding at the outlet of orifice in the PP. In addition, the porous material located behind the PP could hinder the free development of jet at the outlet of orifice, so the flow pattern at the end of the PP is bound to be significantly different from the case without porous material. It may be further conjectured that the jet formed by the large particle velocity at the end of the PP may interfere with the porous layer under certain conditions, and consequently alter the acoustic impedance of the whole structure.

A method of predicting the nonlinear sound absorptive performance of this acoustical unit is proposed as follows. To avoid the difficulty of directly solving the surface acoustic impedance of the whole acoustical unit under a given incident SPL, a calculation procedure from the inner to the outer is adopted. The main solution steps are as follows:

Step 1 Determine the particle velocity u_{ps} under a given sound pressure p_{ps} at the front surface of the porous layer.

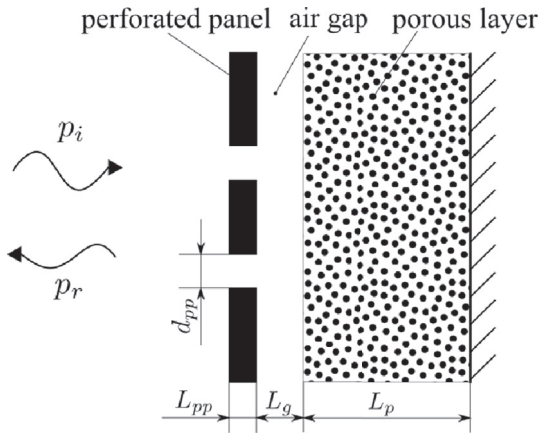

Fig. 1. The acoustical unit of a porous layer with a perforated facing.

Firstly, given an amplitude of the sound pressure at the front surface of the porous layer p_{ps}, some known models and calculation methods [14,18,20–22] can be used to derive the particle velocity at the front surface of the porous layer u_{ps}. Here the corrected form of equivalent complex density proposed by Wilson et al. [14] is used, which has included the Forchheimer-type nonlinear effect. It should be noted that the corrected form of complex density is based on the assumption of pure tones excitation [14]. Meanwhile, based on the results of Wilson et al. [14] and McIntosh et al. [15], it can be assumed that the nonlinear thermal effect could be neglected, that is, the equivalent compressibility is linear. Next, the linearization method and finite difference method are used to solve the differential equation describing the acoustic particle velocity in the porous material, and the details of calculation can be found in Refs. [20,21]. Finally, the particle velocity u_{ps} and surface impedance Z_{ps} at the front surface of the porous layer can be obtained.

Step 2 Derive the sound pressure $p_{\mathrm{pp}-}$ and particle velocity $u_{\mathrm{pp}-}$ at the back surface of the PP.

When the porous layer closely contacts with the PP,

$$p_{\mathrm{pp}-} = p_{\mathrm{ps}}, \quad u_{\mathrm{pp}-} = u_{\mathrm{ps}}\,. \tag{1}$$

When the porous layer is separated from the PP by an air gap with width of L_g,

$$p_{\mathrm{pp}-} = \frac{p_{\mathrm{ps}} + u_{\mathrm{ps}}\cdot Z_0}{2} e^{\mathrm{i}k_0 L_g} + \frac{p_{\mathrm{ps}} - u_{\mathrm{ps}}\cdot Z_0}{2} e^{-\mathrm{i}k_0 L_g}, \tag{2}$$

$$u_{\mathrm{pp}-} = \frac{p_{\mathrm{ps}}/Z_0 + u_{\mathrm{ps}}}{2} e^{\mathrm{i}k_0 L_g} - \frac{p_{\mathrm{ps}}/Z_0 - u_{\mathrm{ps}}}{2} e^{-\mathrm{i}k_0 L_g}, \tag{3}$$

where Z_0 is the characteristic impedance of air, k_0 is the wave number in air, and $\mathrm{i} = \sqrt{-1}$.

When the wavelength of sound is much larger than the width of the air gap, i.e. $\frac{c_0}{f} \gg L_g$, (where c_0 is the sound speed in air and f is the frequency of the sound wave),

$$p_{\mathrm{pp}-} \approx p_{\mathrm{ps}}, \quad u_{\mathrm{pp}-} \approx u_{\mathrm{ps}}\,. \tag{4}$$

Step 3 Calculate the acoustic impedance Z_s of the whole acoustical unit at the front surface of the PP at corresponding incident SPL.

The continuity of volume velocity yields the relationships of the particle velocity in the perforation v_{pp} and at the front surface of the PP $u_{\mathrm{pp}+}$ with the particle velocity at the back surface of the PP

$$v_{\mathrm{pp}} = \frac{1}{\phi_{\mathrm{pp}}} u_{\mathrm{pp}-}, \quad u_{\mathrm{pp}+} = u_{\mathrm{pp}-}\,, \tag{5}$$

where ϕ_{pp} is the perforation ratio of the PP.

When the nonlinear acoustic impedance of the PP is considered, the sound pressure at the front surface of the PP p_{pp+} is represented by

$$p_{pp+} = p_{pp-} + Z_{ppt} u_{pp-}, \tag{6}$$

where Z_{ppt} is the acoustic impedance of the PP, including both linear and nonlinear components, and can be described as

$$Z_{ppt} = \frac{1}{\phi_{pp}} (Z_h + 4R_s + Z_{rad\_out} + Z_{rad\_in}) + Z_{int}, \tag{7}$$

where Z_h is the linear component of acoustic impedance due to the inertia and viscosity of the air layer in a single orifice in the PP; $4R_s$ is the linear component of acoustic resistance owing to the friction loss produced when the air moves along both side surfaces of the PP; Z_{rad_out} is the radiation impedance at the end of a single orifice to the outside (i.e. the side of incident sound waves); Z_{rad_in} is the radiation impedance at the end of a single orifice to the inside (i.e. the side of the porous layer). Both Z_{rad_out} and Z_{rad_in} are linear impedance under low SPL, but under high SPL, the end correction caused by large particle velocity should be considered. Z_{int} is the nonlinear acoustic impedance caused by the PP in the acoustical unit under high sound pressure excitation, including the interference effect between the PP and the porous layer besides the nonlinearity of the single PP (when the interference effect does not exist or can be negligible, Z_{int} is only the nonlinear acoustic impedance of the single PP).

Each term in Eq. (7) is then introduced in more details as follows:

The simplified form of the impedance generated by the viscosity of the air in the orifice Z_h is given by Maa [31]:

$$Z_h = \frac{32\eta L_{pp}}{d_{pp}^2} \sqrt{1 + \frac{x^2}{32}} + i\omega\rho_0 L_{pp} \left(1 + \frac{1}{\sqrt{9 + \frac{x^2}{2}}}\right), \tag{8}$$

where $x = \frac{d_{pp}}{2}\sqrt{\frac{\rho_0\omega}{\eta}}$, ω is the angular frequency, ρ_0 is the density of air, d_{pp} is the diameter of the orifice, η is the dynamic viscosity of air, and L_{pp} is the thickness of the PP.

The linear acoustic resistance owing to the surface friction was given by Rayleigh [32]:

$$R_s = \frac{1}{2}\sqrt{2\omega\rho_0\eta}. \tag{9}$$

Ingard [33] pointed out that the value predicted by this formula is too small compared to the testing result, and Allard [34] proposed that $2R_s$ will give better prediction results. Considering the viscous friction loss at the surfaces on both sides of the PP, $4R_s$ is used in Eq. (7).

The effect of large particle velocity under high SPL on the end correction for the mass of orifice is very complicated, and no simple theoretical formula is available. Maa proposed an empirical correction formula [5], which has a correction factor $\left(1 + \frac{v_{pp}}{\phi_{pp} c_0}\right)^{-1}$ multiplying the linear end radiation impedance of the orifice. This formula has simple form and the predicted value is in good agreement with the experimental results. Here this nonlinear correction factor is used in this study. It is necessary to point out that the correction formula proposed by Maa is only applicable to panels with small perforation ratio and large inter-orifice spacing, the interaction between orifices is not considered, while this interaction is especially significant when the perforation ratio is higher or the inter-orifice spacing is small. In this study, the linear end correction formula proposed by Atalla and Sgard [35] is used, which has considered the interaction between orifices. When air layers exist on both sides of the PP (that is, when an air layer exists between the PP and the porous layer), the nonlinear radiation impedance can be written as

$$Z_{rad\_out} = Z_{rad\_in} = Z_{ae} \left(1 + \frac{u_{pp-}}{\phi_{pp}^2 c_0}\right)^{-1}, \tag{10}$$

where Z_{ae} is the linear end radiation impedance when one side of the PP is the air, and Atalla and Sgard [35] proposed that

$$Z_{ae} = i\omega\rho_0\varepsilon_e, \tag{11}$$

where the length of end correction $\varepsilon_e = 0.48\sqrt{\pi r_{pp}^2}(1 - 1.14\sqrt{\phi_{pp}})$, (where $\sqrt{\phi_{pp}} < 0.4$, and r_{pp} is the radius of orifice).

When one side of the PP closely contacts with the porous layer, it is necessary to consider the influence of the porous layer on the higher-order mode waves radiated by the end of the orifices, and the nonlinear radiation impedance $Z_{\mathrm{rad\_in}}$ to the inside has the following form

$$Z_{\mathrm{rad\_in}} = Z_{\mathrm{pe}}\left(1+\frac{u_{\mathrm{pp-}}}{\phi_{\mathrm{pp}}^2 c_0}\right)^{-1}, \tag{12}$$

where Z_{pe} is the linear radiation impedance of the perforation end on the side of the porous layer, and the formula given by Atalla and Sgard [35] is applied:

$$Z_{\mathrm{pe}} = i\omega\rho\varepsilon_e, \tag{13}$$

where ρ is the equivalent complex density of the porous material. It should be noted that the complex density is used here, rather than the real part of it "Re(ρ)" [35], because the imaginary part of it "Im(ρ)" can consider the influence on the end radiation resistance which have been mentioned before [26,34].

When the particle velocity in the porous material is large, the complex density ρ in Eq. (13) takes the nonlinear form proposed by Wilson et al. [14]:

$$\rho = \rho_p + \frac{\xi\sigma_0\phi|u|}{\sqrt{2}\mathrm{i}\omega}, \tag{14}$$

where ρ_p is the linear equivalent complex density, the velocity u is approximated by the average particle velocity at the front surface of the porous material $u_{\mathrm{pp-}}$, σ_0 is the static flow resistivity of the porous material, and ξ is the Forchheimer's nonlinear parameter of the material.

The nonlinear acoustic impedance Z_{int} under high sound pressure excitation is related to the details of flow pattern in the adjacent regions of perforations. At present, it is difficult to measure the flow field in these small confined regions by experiment, and it is even harder to derive any analytical models. Based on the continuity of volume velocity, the following assumptions are made for the acoustical unit under high SPL excitation. The half period is considered when the particle velocity in the orifice is in the direction towards the porous layer (corresponding to the forward inflow). If an air layer exists between the porous material and the PP, part of the fluid in the jet formed at the end of the orifice will enter the porous material; part of the fluid may be hindered by the material; and vortex may be formed in the air layer between the PP and porous material. If the porous layer is in close contact with the PP, all the air leaving the end of the orifice at high speed will enter the porous material. In contrast, in the other half period when the particle velocity in the orifice is in the direction away the porous layer (corresponding to the backward outflow), the air in the part of porous material close to the orifices will be pumped into the orifices, and jet and vortex may be formed on the opposite end of the orifice. The two conjectured typical flow patterns described above are illustrated in Fig. 2.

The above analysis suggests that firstly, the existence of the porous layer may alter the original jet formation at the end of the orifices in the PP under high sound pressure excitation, further leading to the variation of the nonlinear acoustic impedance of the PP compared to that without the porous layer. Secondly, the local flow velocity of the porous material in the region near the end of the orifices may be increased, and the combined effect of flow viscosity and weak inertia in the porous layer may lead to additional nonlinear loss.

Hence in this study, it is firstly assumed that the distance affected by the interference between the PP and the porous layer is much smaller than the wavelength (the internal flow resistance of the porous material is relatively large, which will suppress the development of jet along the axis). Then it is assumed that the additional nonlinear acoustic impedance caused by the interference effect is equivalent to the changing of nonlinear impedance of the PP in the acoustical unit. The quasi-steady approximation used by Melling [3] in deriving the nonlinear acoustic resistance of the PP is still used in this study (Melling assumed that the acoustic flow through the orifice can be taken to be quasi-steady, and correspondingly, the nonlinear acoustic resistance induced by the kinetic energy loss can be expressed by the pressure loss of steady flow through the orifice). Melling has given the nonlinear acoustic resistance of a single PP, which can be written as

$$R_{\mathrm{nl}} = \frac{8K_f}{3\pi\phi_{\mathrm{pp}}^2}|u_{\mathrm{pp-}}| = \frac{8}{3\pi}K_{\mathrm{pp}}|u_{\mathrm{pp-}}|, \tag{15}$$

where K_f is the effective mass density parameter [3], which is related to the geometry of orifice and perforation ratio. For a single orifice, it may be expressed as a function of the discharge coefficient and reflects the significance of the nonlinearity of a PP. Here "$K_{\mathrm{pp}} = K_f/\phi_{\mathrm{pp}}^2$" is the velocity coefficient of the specific flow resistance of a PP (refer to subsection 3.1.1 for more details). It can be obtained by measuring the pressure loss of steady flow passing through a PP. It should be pointed out that the above quasi-steady model of nonlinear acoustic resistance of a PP is based on the assumption of pure tone excitation, which implies that the nonlinear harmonic interaction or the cross-coupling effects cannot be considered in the quasi-steady model when the acoustic excitation contains multiple harmonics or is random [36,37].

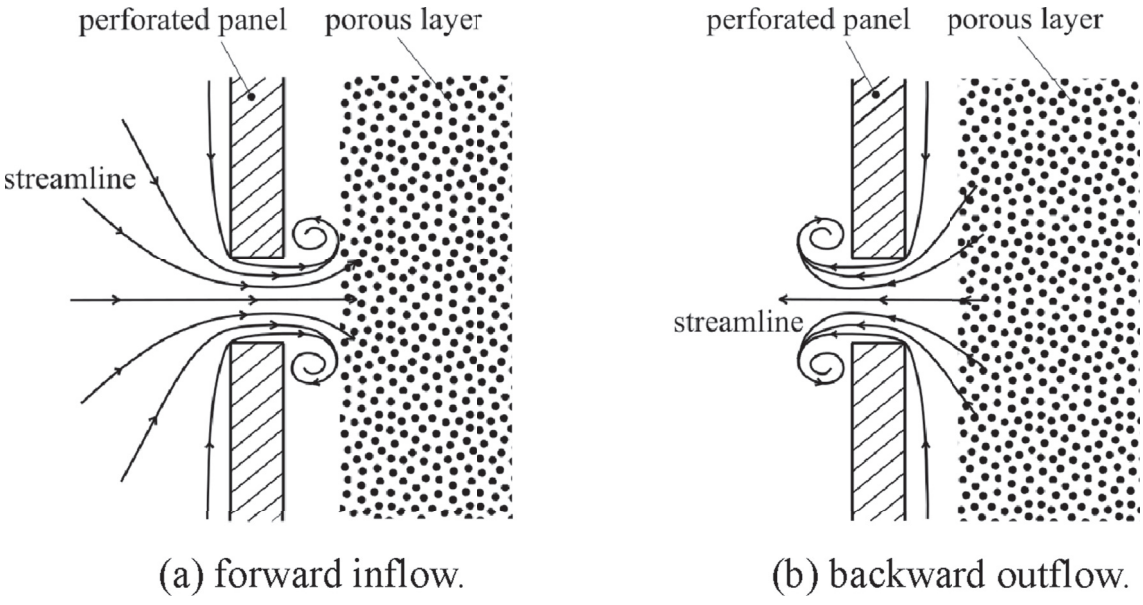

Fig. 2. Schematic illustration of the conjectured typical flow patterns of the acoustical unit at high sound pressure excitation.

Similar to the form of the nonlinear acoustic resistance of a PP proposed by Melling, here it is assumed that with the introduction of the porous layer, the nonlinear acoustic resistance of a PP in the acoustical unit can still be represented by the parameters corresponding to the pressure loss across the PP when a steady flow passes through the whole unit, i.e.

$$R_{\text{int}} = \frac{8}{3\pi} K'_{\text{pp}} |u_{\text{pp}-}|, \tag{16}$$

where K'_{pp} is the velocity coefficient of the specific flow resistance of the PP in the acoustical unit under the corresponding condition. This parameter can be determined by testing the difference between the specific flow resistance of the acoustical unit and that of the single porous layer, and more details are described in subsection 3.2.2. Note that the influence of the interference effect on the nonlinear acoustic reactance cannot be included here, because it depends on more details of the complex flow and can hardly be described mathematically.

After each term in Eq. (7) is determined, the acoustic impedance of the PP Z_{ppt} is obtained. Then Eq. (6) is used to calculate the sound pressure at the front surface of the PP, and the surface acoustic impedance of the whole acoustical unit is calculated as follows:

$$Z_s = Z_{\text{pp}+} = \frac{p_{\text{pp}+}}{u_{\text{pp}+}}. \tag{17}$$

The amplitude of the incident sound pressure at the front surface of the PP is calculated by

$$|p_i| = \left| \frac{p_{\text{pp}+}}{2} \left(1 + \frac{Z_0}{Z_s} \right) \right|. \tag{18}$$

By giving a set of stepwise increasing sound pressures at the front surface of the porous layer, and following the three above calculation steps, the sound absorptive performance of the whole acoustical unit under varying incident SPLs can be predicted. It should be emphasized that the prediction model proposed above is restricted to pure tone excitation, because both the corrected form of complex density of porous material by Wilson and the quasi-steady form of nonlinear resistance of PP by Melling (which are adopted here) are based on the assumption of pure tone excitation as mentioned above. Besides, the above-proposed model is restricted to a rigid-frame porous media; therefore, if the frame of the porous layer is not rigid, then different models, based on elastic-frame assumption, may need to be developed.

3. Experimental validation and discussions

The prediction model proposed in Section 2 mainly requires the following parameters of porous material: the linear characteristic impedance Z_p, complex wave number k_p, linear static flow resistivity σ_0, Forchheimer's nonlinear parameter ξ,

and thickness of the porous layer L_p. Among these parameters, Z_p and k_p can be derived from a linear acoustic model of porous material or measured by acoustical experiments. At present, not all of the parameters in the linear acoustic model of porous material can be directly measured in our laboratory, so the transfer matrix method [38] is used to measure Z_p and k_p. A flow resistance testing device is used to measure the parameters σ_0 and ξ of the porous material. The velocity coefficient of the specific flow resistance of the PP K'_{pp} in Eq. (16) is also measured with the same device.

In order to validate the proposed prediction model, an impedance tube is established to test the sound absorptive performance of the acoustical unit under different incident SPLs.

3.1. Testing systems

A brief introduction of the flow-resistance-testing device and the impedance tube is presented in this subsection.

3.1.1. Static flow resistance measurement

The tested acoustical unit sample is fixed by a holder shown in Fig. 3. The holder is connected with the upstream and downstream static pressure testing tube via fastening thread. The holder has inner diameter of 29 mm (the same as the inner diameter of the impedance tube used in the sound absorption test). In order to fix the perforated facing, the outer diameter of the perforated facing is designed to be 33.5 mm, slightly larger than the inner diameter of the holder, and the boundary condition of the perforated facing is approximately being peripherally clamped. The width of the air gap between the PP and porous material can be adjusted by a set of positioning rings with different thicknesses.

In the experiment, the static pressure difference across the acoustical unit can be measured when a steady flow passes through the structure in the forward and backward directions. The airflow is driven by an air compressor, and the static pressure differences across the testing samples are determined by a set of differential manometers with different measurement ranges. The flow rate passing through the material or structure is controlled by a mass flow controller, and the control range of the mean steady flow velocity passing through the cross section of the material U_{dc} is 0.016–0.81 m/s in the experiment.

When the average flow velocity in a porous material is large enough, the static flow resistivity of the porous material approximately satisfies the Forchheimer's law [18], and the static flow resistivity can be written as

$$\sigma = \sigma_0(1 + \xi|U_{dc}|), \tag{19}$$

where the parameters σ_0 and ξ can be obtained by linear regression of the results of the flow resistance experiment.

Correspondingly, the specific flow resistance of the porous material layer is defined as [39].

$$R_p \equiv \frac{\Delta p}{U_{dc}} = \sigma L_p = \sigma_0 L_p + K_p|U_{dc}|, \tag{20}$$

where Δp is the static pressure difference across the sample when the airflow passes the sample, K_p is the velocity coefficient of the specific flow resistance of porous layer.

When the mean flow velocity passing through a single PP is large enough, the relationship between its specific flow resistance R_{pp} and the velocity is also approximately linear [3], and can be described as

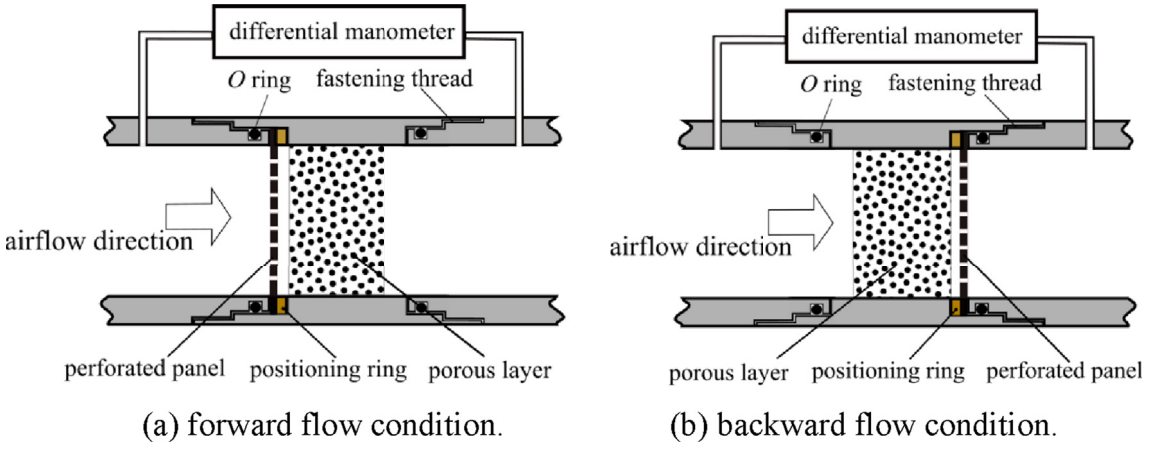

Fig. 3. Schematic illustration of the test rig for measuring the flow resistance of the acoustical unit.

$$R_{pp} \equiv \frac{\Delta p}{U_{dc}} = R_{pp0} + K_{pp}|U_{dc}|, \tag{21}$$

where the velocity coefficient K_{pp} can be obtained by linear regression of the specific flow resistance of the single PP, and R_{pp0} is the linear viscous resistance.

In order to investigate the influence of the additional resistance brought by the interference between the PP and the porous layer at high flow velocity, the flow resistance of the whole acoustical unit is measured as

$$R_c \equiv \frac{\Delta p}{U_{dc}}. \tag{22}$$

For different widths of air gap between the PP and the porous layer, the flow resistances in the forward flow direction are tested. For the PP in close contact with the porous layer, the specific flow resistance is tested when steady flow passes through the acoustical unit in the forward and backward flow directions alternately.

3.1.2. High-SPL sound absorption measurement

The sound absorptive performance of the acoustical unit under high SPL is tested in the impedance tube setup shown in Fig. 4. The test principle is based on the two-microphone transfer function method [40]. The sound source uses a 400 W compression driver BMS 4599 with an audio power amplifier KUDO MA7200s. A B&K 3160 front-end is used for signal generator and data acquisition, and two 1/4-inch B&K 4944 pressure-field type microphones with the effective upper limit of dynamic range of 169 dB are flush mounted on the wall. The impedance tube is built up by using a designed transitional tube connecting the sound source and a B&K 4206 small measurement tube. The inner diameter of the impedance tube is 29 mm and the microphone spacing is 20 mm, which determines the effective range of testing frequency to be 500 Hz–6.4 kHz. In the experiment at a given excitation frequency, the amplitude of the input signal of the power amplifier is gradually increased to improve the incident SPL at the surface of testing sample, and the sound absorptive performance at different incident SPLs are measured.

As shown in Fig. 4, the transfer function H_{12} [40] is defined as

$$H_{12} = \frac{p_2}{p_1}, \tag{23}$$

where p_1 and p_2 are sound pressures in the two microphone positions.

The reflection coefficient [40] can be expressed as

$$r = \frac{H_{12} - e^{-ik_0 s}}{e^{ik_0 s} - H_{12}} e^{2ik_0 x_1}, \tag{24}$$

where $s = x_1 - x_2$, which is the distance between the acoustic centers of the two microphones. The normalized specific surface acoustic impedance [40] is

$$z_s = \frac{Z_s}{Z_0} = \frac{1+r}{1-r}. \tag{25}$$

The sound absorption coefficient [40] is

$$\alpha = 1 - |r|^2. \tag{26}$$

The complex magnitude of the incident sound pressure on the structure surface is

$$\widehat{p}_I = \frac{p_1 e^{-ik_0 x_2} - p_2 e^{-ik_0 x_1}}{2i\sin(k_0 s)} = \frac{p_1\left(e^{-ik_0 x_2} - H_{12} e^{-ik_0 x_1}\right)}{2i\sin(k_0 s)}. \tag{27}$$

The incident SPL is defined as

$$L_{p_i} \equiv 20\lg \frac{|\widehat{p}_I|}{\sqrt{2} p_{ref}}, \quad p_{ref} = 2.0 \times 10^{-5}\mathrm{Pa}. \tag{28}$$

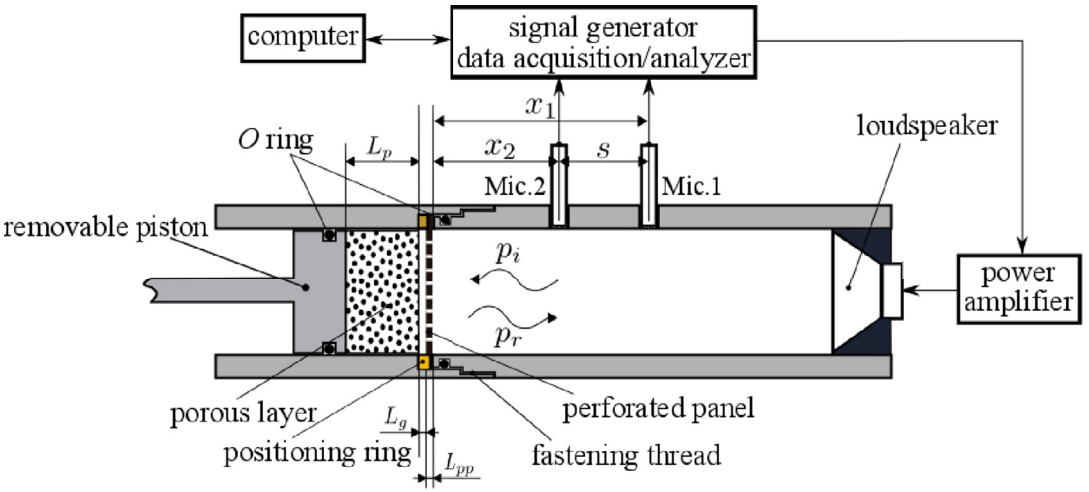

(a) schematic illustration of the impedance tube.

(b) photo of the impedance tube.

(c) photo of the amplifier and the data acquisition front-end.

Fig. 4. The impedance tube for measuring the sound absorption of the acoustical unit under varying excitation SPLs.

3.2. Results and discussions

3.2.1. Testing samples

In order to validate the model proposed in Section 2 for predicting the sound absorption of an acoustical unit, experiments are conducted on units alternately formed by the combination of three stainless steel PPs with different perforation ratios and with the same piece of sintered metallic fibers (SMF) material backed by rigid wall. The specific parameters of the PP are shown in Table 1. The orifices of the PPs are distributed as uniformly as possible in equilateral triangles, and have square edges at the inlet and outlet. The thickness of the SMF sample is 15 mm and the porosity is 0.85. It has been known that the

Table 1
Basic parameters of the perforated panels.

Facing number	Orifice diameter d_{pp}(mm)	Plate thickness L_{pp} (mm)	Perforation ratio ϕ_{pp}
PP1	2	0.9	0.0476
PP2			0.0904
PP3			0.228

nonlinearity of a PP is determined by the perforation ratio, aperture, panel thickness and the shape of orifice edge [3]. In the experiment, only the perforation ratio of PP is chosen as a parameter for comparison, mainly because the perforation ratio has the most significant effect on the nonlinear behavior of a PP (refer to the test results by Melling [3]). It is necessary to point out that under the linear condition generally when the perforation ratio is above 0.2, the facing panel will have small influence on the surface impedance of the porous layer [34,41], so wideband absorptive performance of porous material at middle-to-high frequencies can be maintained. Consequently, a perforated panel "PP3" with a higher perforation ratio (22.8%) is also chosen in the experiment. However, the increase of perforation ratio will also reduce the mechanical stiffness of the facing panel, so the requirements of acoustical performance and structural mechanical property often need to be balanced in practical applications. The thicknesses and orifice diameters of all the three PPs are fixed to be 0.9 mm and 2 mm, respectively, as commonly used in practice.

3.2.2. Results and analysis of static flow resistance experiment

In the static flow resistance experiment, the results of the SMF sample are as follows: $\sigma_0 = 14137\text{Pa}\cdot\text{s/m}^2$, $\xi = 0.581\text{s/m}$, and $K_p = 168\text{kg/m}^3$; the results obtained from the forward and backward flow conditions are almost equal. The measured velocity coefficients of the specific flow resistance of the PP samples (K_{pp}) are listed in Table 2, and the results show that the coefficient significantly decreases with the increase of perforation ratio. For comparison, the sums of K_p and K_{pp} for each combination are also listed in Table 2. The data in Table 2 show that the velocity coefficients of the three PPs are larger than, close to, or smaller than that of the SMF sample. The velocity coefficient of the specific-flow resistance reflects the nonlinear effect of the flow passing through the sample.

The flow resistance in the presence of forward flow through the acoustical unit is measured when an air gap with different widths ($L_g = 0.1, 0.2, 0.3, 0.5, 1, 2\text{mm}$) lies between the PP and the porous layer. Moreover, when the PP is in close contact with the porous layer, the flow resistance of the acoustical unit is measured when a steady flow passes through the structure in both forward and backward directions. The test results are shown in Fig. 5, and the "+D." and "-D." labels in the graphs represent the forward and backward flow conditions, respectively, and the abbreviation "PP+SMF" in the figure caption represents the acoustical unit composed of the SMF sample covered with corresponding perforated panel, such as PP1. For the convenience of comparison, the sum of the specific flow resistances of the SMF sample and the PPs after linear fitting is plotted in Fig. 5 (labeled by "sum"), and the measured specific flow resistance of the SMF sample and PP samples are also plotted in the figure.

Fig. 5 indicates that the specific flow resistance of the whole acoustical unit also has an approximately linear relationship with the flow velocity:

$$R_c \equiv \frac{\Delta p}{U_{\text{dc}}} = R_{c0} + K_c|U_{\text{dc}}|, \tag{29}$$

where K_c is the velocity coefficient of the specific flow resistance of the acoustical unit, and R_{c0} is the linear viscous resistance. The velocity coefficients of the three acoustical units in the corresponding state are listed in Table 2. Note that the velocity coefficient of the PP in the acoustical unit K'_{pp} in Eq. (16) (describing the nonlinear acoustic resistance of the PP in the acoustical unit) is the slope of the linear fitting straight line describing the difference between the specific flow resistance of the whole acoustical unit and that of the porous material layer, i.e. the difference between formula (29) and (20) ($R_c - R_p$) vs. the flow velocity U_{dc}.

Table 2
The measured velocity coefficient of specific flow resistance of the samples (kg/m^3).

Facing number	Velocity coefficient of the specific flow resistance of the acoustical unit K_c								K_{pp}	$K_{pp} + K_p$
	Air gap thickness L_g (mm)									
	0 (-D.)	0	0.1	0.2	0.3	0.5	1	2		
PP1	1437	941	888	722	643	637	658	669	482	650
PP2	484	360	339	308	294	292	293	288	116	284
PP3	225	205	198	195	194	190	189	181	13.9	182

(Note: "-D." represents the backward flow condition, and others belong to the forward flow condition.).

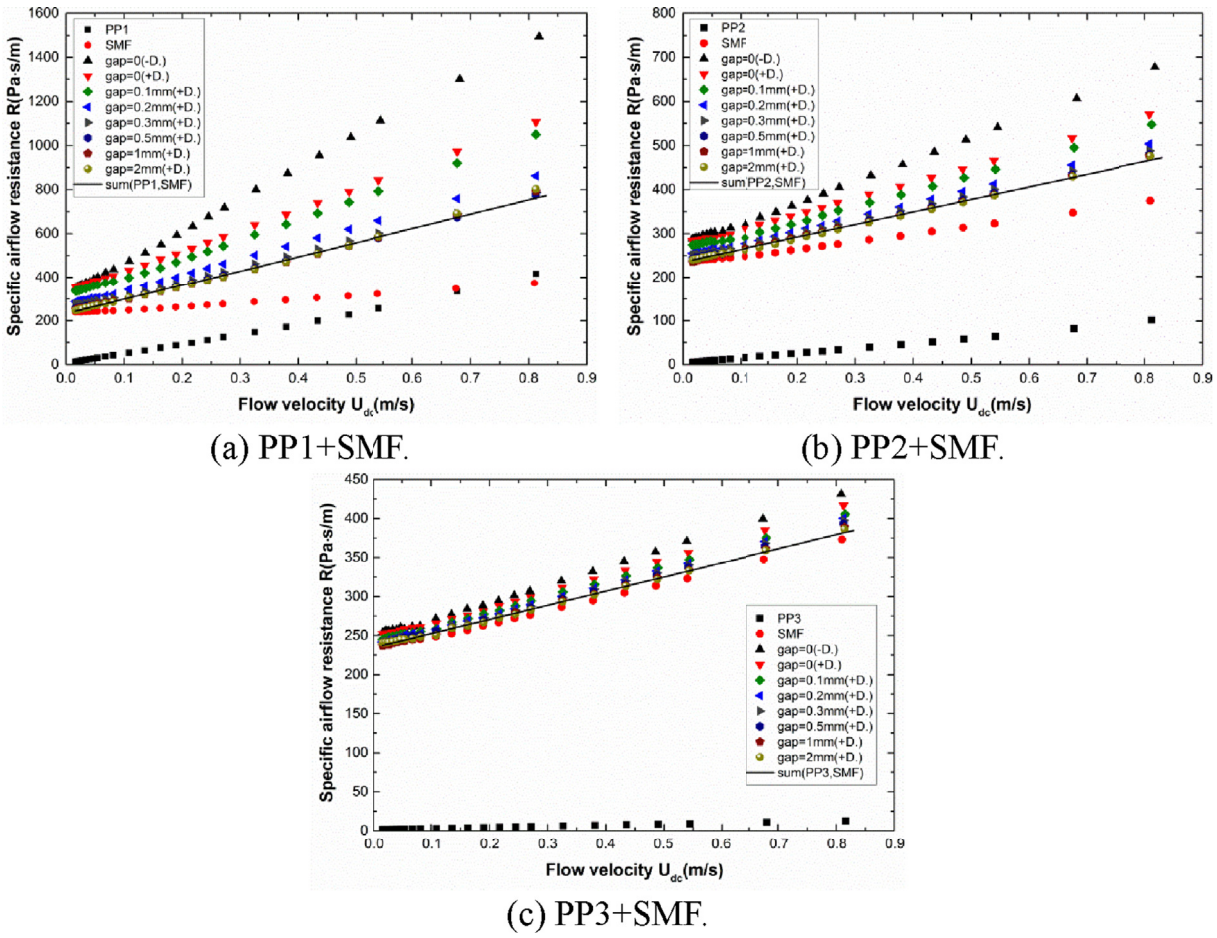

Fig. 5. Results of the measured specific flow resistance of the acoustical unit.

It can be seen from Table 2 and Fig. 5 that when the backward flow passes through the acoustical unit, the velocity coefficient of flow resistance of the structure containing PPs with small perforation ratios is significantly higher than that in the presence of forward flow. Moreover, with the increase of perforation ratio, the difference between the two flow conditions is gradually reduced. These phenomena involve details about the complex flow in the acoustical unit, and further theoretical analysis is required. In the presence of forward flow through the acoustical unit, with the increase of the air gap between the PP and porous material layer, the total specific flow resistance of the acoustical unit gradually decreases and approaches the sum of the specific flow resistance of the SMF sample and the PP. When the air gap width is kept constant, the specific flow resistance of the unit consisting of PPs with higher perforation ratios is closer to the sum of the specific flow resistance of the SMF sample and the PP. Therefore, it can be inferred that the smaller is the perforation ratio of the PP, and the smaller is the width of the air gap, the stronger the interference effect becomes.

For different air gap widths, the increment of the velocity coefficient of the specific flow resistance of the acoustical unit is defined as

$$\Delta K \equiv K_c - (K_p + K_{\mathrm{pp}}), \tag{30}$$

where ΔK reflects the increment of nonlinear resistance owing to the interference between the panel and the porous layer. Fig. 6 shows the experimental data and the curves fitted using the exponential function "$\Delta K = \Delta K_0 + A \cdot e^{-B \cdot L_g}$". It can be seen that the increment of the velocity coefficient decreases with the increase of the air gap width in an approximately exponential function.

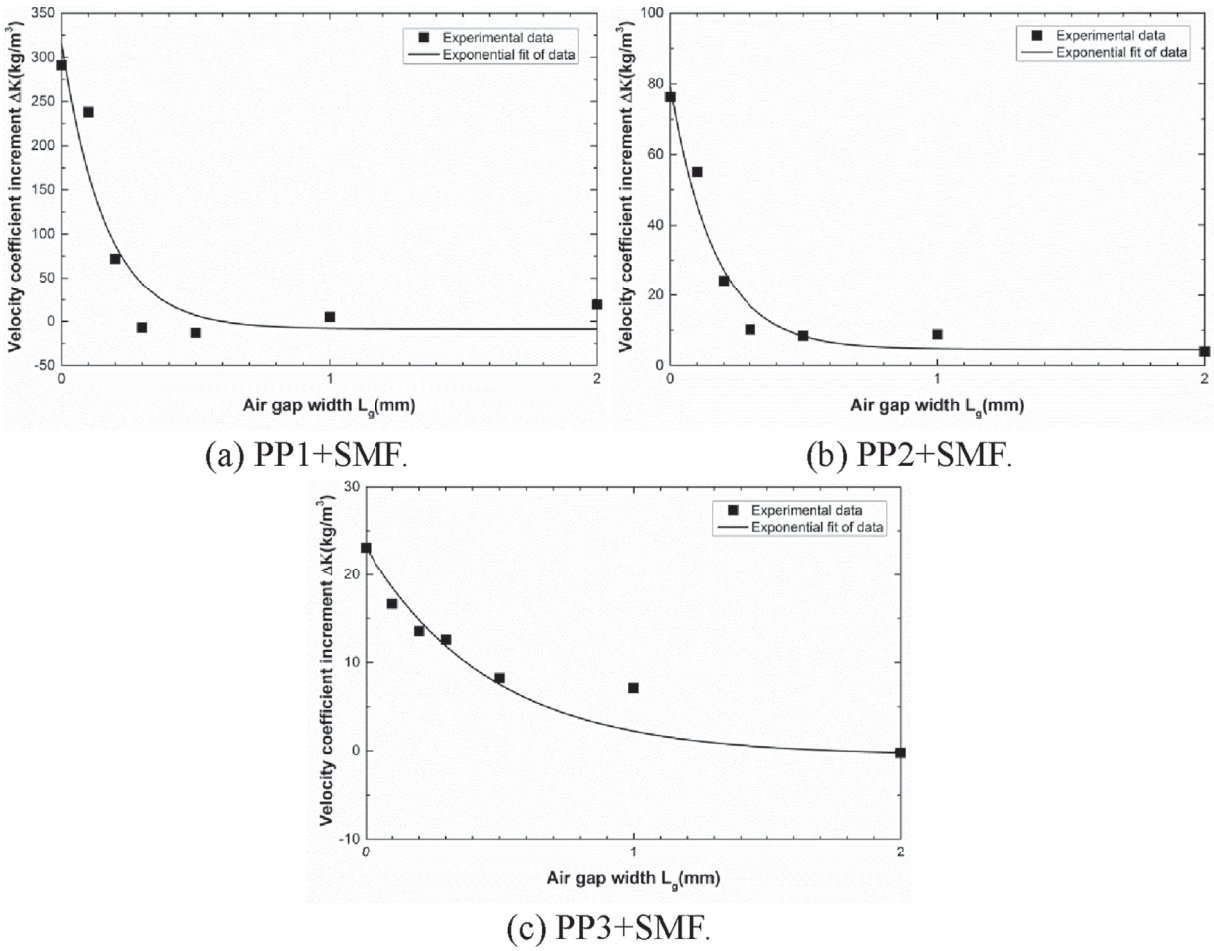

Fig. 6. Variation of the increment of velocity coefficient of specific flow resistance with the air gap width between the PP and the porous layer.

3.2.3. Comparison of sound absorption under linear condition

The linear model for the acoustical unit is checked firstly. The sound absorptive performance of the three above-mentioned acoustical units is tested at low SPL (i.e. under linear conditions). The samples are tested with rigid backing in two configurations: 1) the PP in contact with the porous layer; 2) an air gap with width of "$L_g = 0.5$mm" separating the porous layer and the PP.

The linear characteristic impedance and complex wave number of the SMF sample required in the theoretical model are measured with the transfer matrix method [38], and the test results are shown in Fig. 7.

When the PP is in close contact with the porous layer, the measured and predicted results are shown in Fig. 8. The plots show that the predicted results agree well with the measured data. Additionally, when the perforation ratio is increased up to 22.8%, the predicted and measured sound absorption coefficient deviate a little from each other (the relative large error exists in the frequency range of 3.2~6k Hz, among which the maximum error is about 0.07), probably because the approximation formula of the correction length requires "$\phi_{pp} < 0.16$" [34], which is less satisfied in case of higher perforation ratio.

When an air gap with width "$L_g = 0.5$ mm" lies between the PP and the porous layer, the measured and predicted results are shown in Fig. 9. The results show that the predicted values are in overall good agreement with the measured values, and the predicted sound absorption is slightly lower than the measured value for the panel with low perforation ratio. The reason may be that in the prediction model, the end correction on the side of the PP facing the air gap adopts the same form as that of

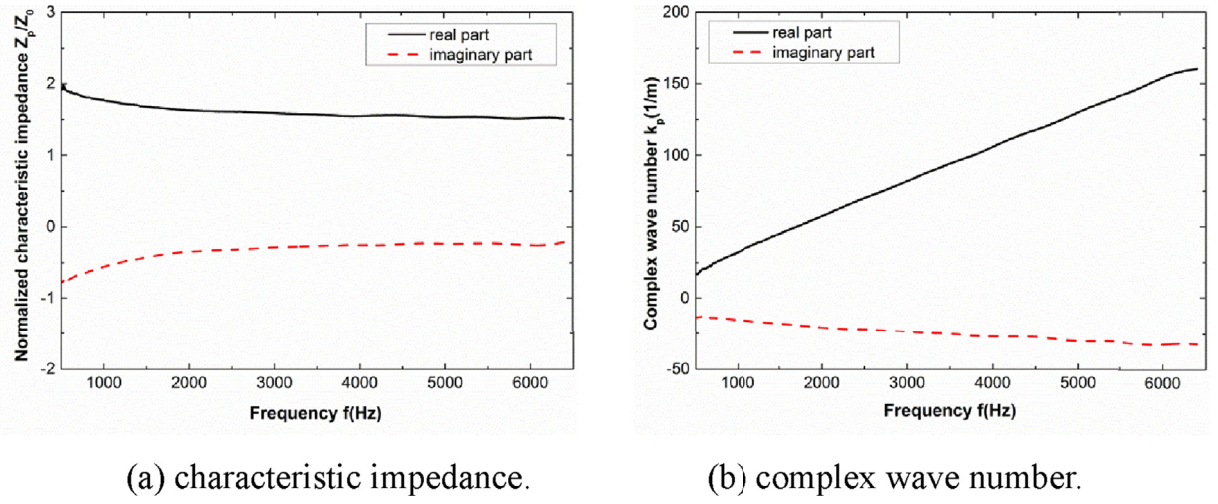

Fig. 7. Measured results of the characteristic impedance and complex wave number of the SMF sample.

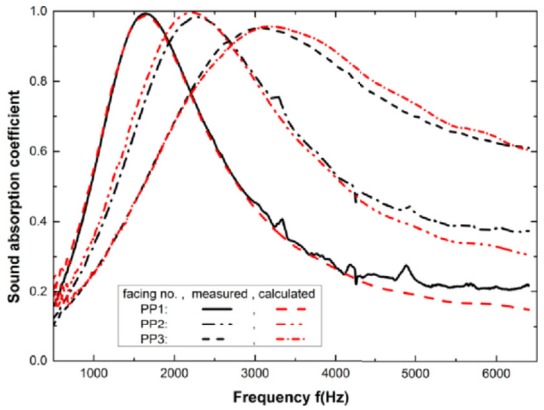

Fig. 8. Comparison of the measured and predicted results of sound absorption coefficient of acoustical units for the configuration of the PP in contact with the porous layer.

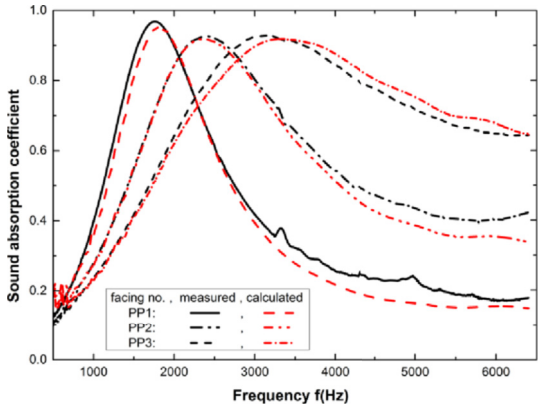

Fig. 9. Comparison of the measured and predicted results of sound absorption coefficient of acoustical units for the configuration of an air gap with width of L_g = 0.5mm separating the porous layer and the PP.

the side facing the air, while the porous layer may still alter the end radiation resistance of the orifice, in spite of the existence of 0.5-mm-wide air gap.

Both the above cases also indicate that, with the increase of perforation ratio of the panel, the peak of sound absorption gradually moves to a higher frequency; meanwhile, the bandwidth of sound absorption gradually broadens. The main reason is that with the increase of perforation ratio, the effect of the additional acoustic impedance caused by the PP is gradually reduced, and the sound absorptive performance of the acoustical unit is closer to that of the porous layer. Similar trend of variation has been mentioned and analyzed before [34].

3.2.4. Comparison and analysis of sound absorption at high SPLs

To corroborate the validity of the prediction model developed in Section 2, the sound absorptive performance of the three above-mentioned acoustical units is tested under the incidence of different SPLs. Firstly, the samples are also tested in the two configurations with hard wall backing mentioned in Section 3.2.3. In the experiment, three typical excitation frequencies are chosen for each acoustical unit: one is close to the linear resonant frequency of the structure, and the other two are below and above the linear resonant frequency, respectively. At each excitation frequency, the incident SPL is increased stepwise, and the surface acoustic impedance and sound absorption coefficient of the structure are measured. Lastly, corresponding measurements are made under the condition when an air cavity is set between the porous material and the hard backing wall for the configuration of the PP3 in contact with SMF. It should be emphasized that, because of the limitation of the loudspeaker (its power and frequency-response characteristics), the maximum incident SPL in the experiment (which is also dependent on the surface impedance of testing sample) cannot all be attained up to be 160 dB for each excitation frequency and each configuration, while the predicted results are given for the cases up to 170 dB, with the aim of providing theoretical references for the varying trends.

For the two configurations with hard wall backing as mentioned above, the experimental results and theoretical predictions are compared for the three acoustical units under excitation at near resonant frequency in Figs. 10 and 11.

3.2.4.1. Nonlinear impedance for the configuration when the PP is in contact with the porous layer. (a) Nonlinear acoustic resistance. The nonlinear acoustic resistance caused by the interference between the PP and the porous layer is calculated in two different ways: 1) inserting the velocity coefficient of specific flow resistance of the PP measured when a forward flow passes through the acoustical unit in Eq. (16) yields the results labeled “mod1” in Fig. 10; 2) inserting the mean value of the velocity coefficients of specific flow resistance in the presence of a forward and a backward flow passes through the acoustical unit in Eq. (16) yields the results labeled “mod2” in Fig. 10. The nonlinear acoustic resistance predicted with the interference effect neglected, i.e. just taking the nonlinear acoustic resistance of a single PP R_{nl} in Eq. (15), is also shown in the figure. The results show that at the incidence of high SPL, the surface specific resistance predicted with the interference effect neglected is significantly lower than the experimental result, especially for the combination containing panel with small perforation ratio (such as PP1). Moreover, with the increase of the incident SPL, the difference between the two values above also tends to increase gradually. Hence, it can be inferred that the interference effect will induce more significant variation in the nonlinear acoustic resistance of combinations containing panel with smaller perforation ratio. The predicted specific surface acoustic resistance corresponding to mod1 is much closer to the measured data; correspondingly, the predicted absorption coefficient is also closer to the measured value. On the other hand, at the incidence of high SPL, the predicted resistance corresponding to mod2 is slightly higher than the measured value, which means that the increment of specific flow resistance in the backward flow condition overestimating the nonlinear acoustic resistance caused by interference under the excitation of high SPL (corresponding to the half period when the particle velocity in the orifice is in the direction away the porous layer). Further theoretical investigations are needed to explain this phenomenon.

(b) Nonlinear acoustic reactance. The acoustic reactance predicted by the models decreases monotonously with the increase of the incident SPL. The overall trend of predicted reactance is similar to that of the experimental results, but some deviation still exists. Moreover, for the units containing panels with smaller perforation ratio such as the PP1 panel, the measured acoustic reactance gradually approaches to a constant when the incident SPL reaches a critical value in the range of 150–160 dB (this phenomenon is similar to the nonlinear behavior of acoustic reactance found in the early study conducted by Melling [3] on the acoustic properties of a PP at high SPL. He found that at high SPL, the acoustic reactance of a PP gradually approaches to a constant, the asymptotic value of about half of the linear value). The main cause of the deviation between the predictions and the measurements may be due to the additional nonlinear acoustic reactance, generated by the interference effect, which has not been considered in the prediction model.

3.2.4.2. Nonlinear impedance for the configuration when a 0.5-mm-wide air gap lies between the PP and porous layer. (a) Nonlinear acoustic resistance. The velocity coefficient of specific-flow resistance of the perforated panel measured in the presence of forward flow is used to calculate the nonlinear acoustic resistance R_{int} in Eq. (16) (corresponding to the predicted results labeled with “mod1” in Fig. 11), and the nonlinear acoustic resistance predicted with the interference effect

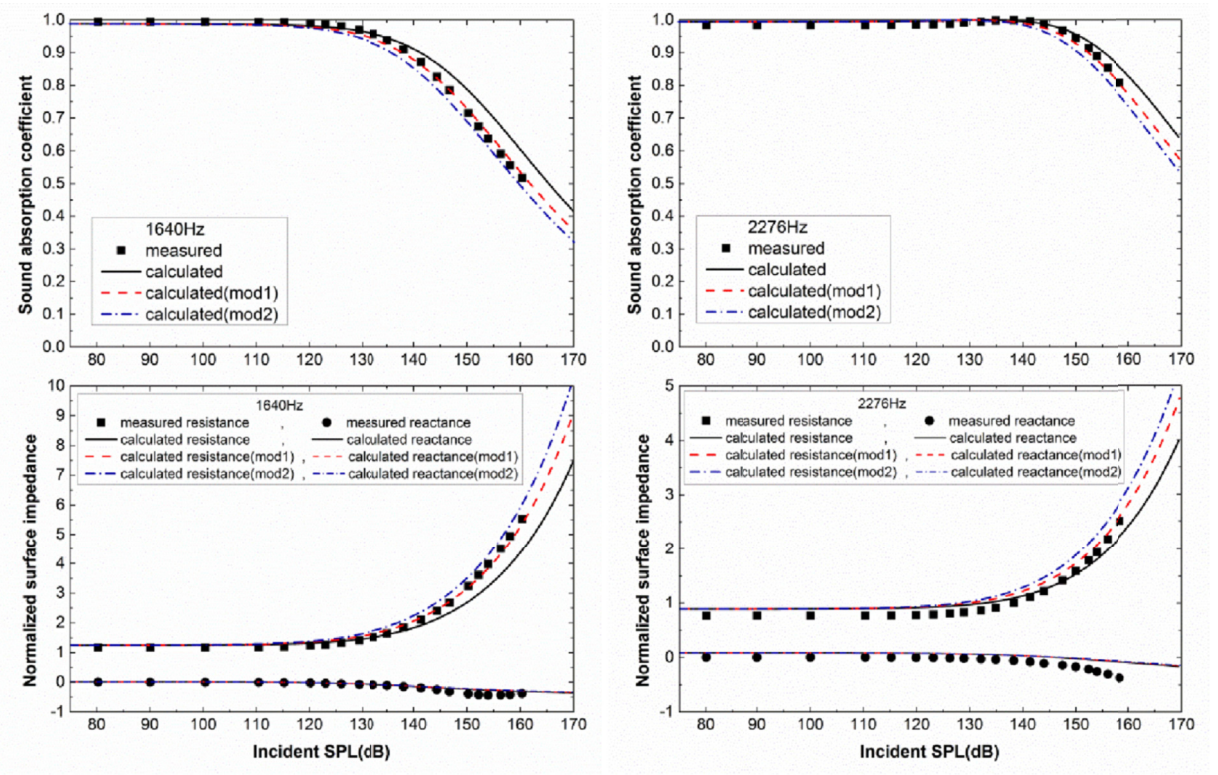

(a) PP1+SMF. (b) PP2+SMF.

(c) PP3+SMF.

Fig. 10. Comparison of the measured and predicted results of sound absorption and surface impedance of acoustical units under different incident SPLs for the configuration of the PP in contact with the porous layer.

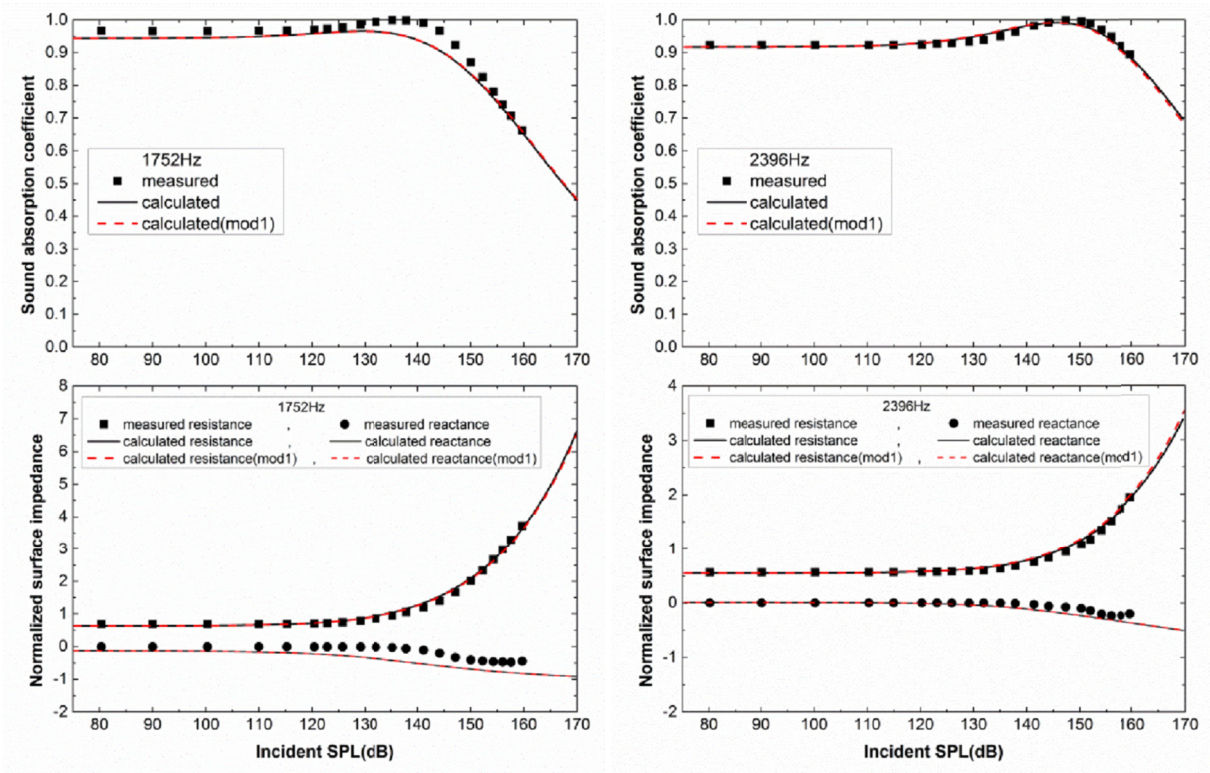

(a) PP1+SMF. (b) PP2+SMF.

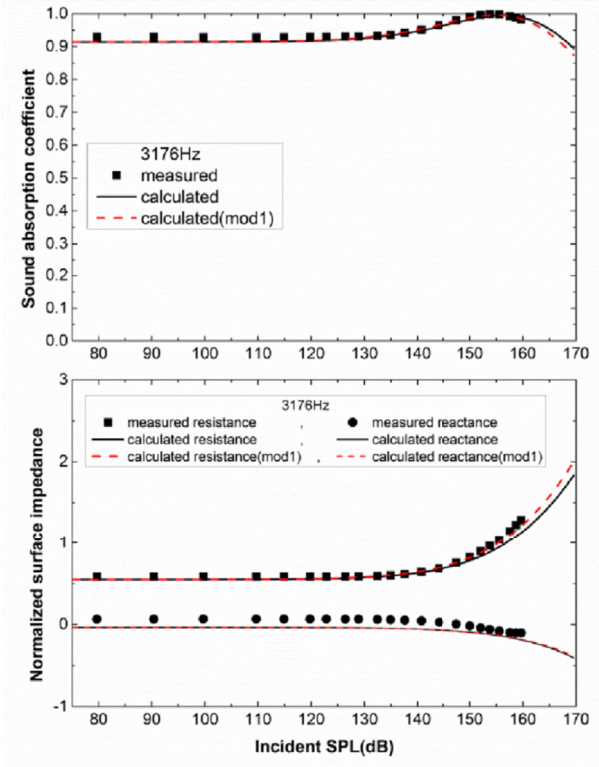

(c) PP3+SMF.

Fig. 11. Comparison of the measured and predicted results of sound absorption and surface impedance of acoustical units under different incident SPLs for the configuration of an air gap with width of $L_g = 0.5$mm separating the porous layer and the PP.

neglected is also shown in the figure. The results show that for the acoustical units with panel PP1 and PP2, the results predicted with the two methods are very close, suggesting that the variation of nonlinear acoustic resistance induced by interference is relatively small. This is mainly because the introduction of 0.5-mm-thick air layer significantly reduces the interference effect. The test results of the specific flow resistance for the acoustical units support this statement: the increment of velocity coefficient of the acoustical unit is small relative to the velocity coefficient of the single PP ($\Delta K/K_{pp}$ are 0.027 and 0.069 for PP1 and PP2, respectively), so the increase of nonlinear acoustic resistance induced by interference effect can be neglected for the two cases. For the acoustical unit containing the PP3 panel, the acoustic resistances predicted with the two methods show deviation starting from 150 dB, and the difference gradually increases with the increase of SPL. Among these results, the predictions based on mod1 are closer to the experimental results. The test results of specific flow resistance show that although the introduction of air gap makes the increment of velocity coefficient significantly lower than the value when the PP is in contact with the porous layer, it is still large relative to the velocity coefficient of the single PP ($\Delta K/K_{pp} = 0.65$), hence the increment of nonlinear acoustic resistance caused by interference cannot be ignored for this case.

(b) Nonlinear acoustic reactance. The experimental results show that the specific acoustic reactance also gradually approaches to a constant value with the increase of SPL. Under some conditions (such as combinations containing the panel PP1), relatively large difference exists between the predicted and measured acoustic reactance under high SPL. Hence, although good agreement is found between the predicted and measured acoustic resistance, relatively large difference is found between the corresponding predicted and measured absorption coefficient.

The results of nonlinear sound absorption of the acoustical unit in the above two configurations show that, similar to the sound absorptive characteristics of a single porous layer [14,22] and a perforated panel [5], the sound absorptive performance of the acoustical unit also has two typical trends with the incident SPL, corresponding to the over-resistance state and the under-resistance state. The over-resistance state corresponds to the relative surface acoustic resistance of the structure of greater than 1 at resonance under linear condition, and the absorption coefficient will monotonously decrease with the increase of SPL. For example, the experimental results of the acoustical unit consisting of the PP1 in contact with the SMF sample show that the linear relative surface resistance of the structure is 1.2 near resonance, and when the SPL reaches 150 dB, the sound absorption coefficient has been reduced from 0.99 to 0.72. The under−resistance state corresponds to the relative surface acoustic resistance of the structure of less than 1 at resonance under linear condition, and the sound absorption coefficient will increase with the incident SPL to a maximum value and then decrease gradually. The experimental results show that after the introduction of a 0.5-mm-thick air layer between the PP1 panel and SMF sample, the linear relative surface resistance of the structure becomes 0.69 near resonance; when the incident SPL reaches about 140 dB, the sound absorption coefficient is close to the maximum value of total absorption; when the SPL is further increased to 150 dB, the sound absorption coefficient is reduced to 0.87. It can be seen that the structure designed to be in an under-resistance state under linear condition can effectively broaden the range of SPL of high sound absorption. Comparison of different combinations of perforated panel shows that with the increase of perforation ratio, the critical SPL corresponding to the maximum sound absorption coefficient near resonance increases gradually, mainly because the additional acoustic resistance brought by a PP with larger perforation ratio is smaller and the under-resistance characteristic of the structure is more significant.

To demonstrate the effect of excitation level on the absorption more clearly, Fig. 12 shows the predicted sound absorption coefficients of the acoustical units against the frequency for various incident SPLs (labeled by “calculated”), and the corresponding experimental data (labeled by “data”). The experimental data consists of the result near the resonant frequency (as shown in Figs. 10 and 11) and the results at two other frequencies, one below and the other above the resonant frequency. It should be noted that, the marker “NA” in the legend of Figs. 12 and 13 represents that the corresponding data is not available by measurements. In the figure, the predicted results generally agree well with the experimental data. It can also be noticed that some deviation exists between the predicted results and the experimental data, especially at those non-resonant frequencies; this is mainly because the prediction model has not considered the additional nonlinear acoustic reactance generated by the interference effect, which has been discussed above. Besides, the deviation between the predicted results and the data under the linear condition (which has been described in subsection 3.2.3) is also reflected in Fig. 12. The absorption curves also display the trend of absorption bandwidth broadening with the increase of incident SPL regardless the state of the acoustical unit (over-resistance or under-resistance).

Fig. 13 shows the results for the condition when an air cavity with 60 mm in depth is set between the porous material and the hard backing wall for the configuration of the PP3 in contact with SMF. The results show that, with the increase of incident SPL, the absorption peak of each order first increases to a maximum and then decreases, while the absorption band gradually broadens.

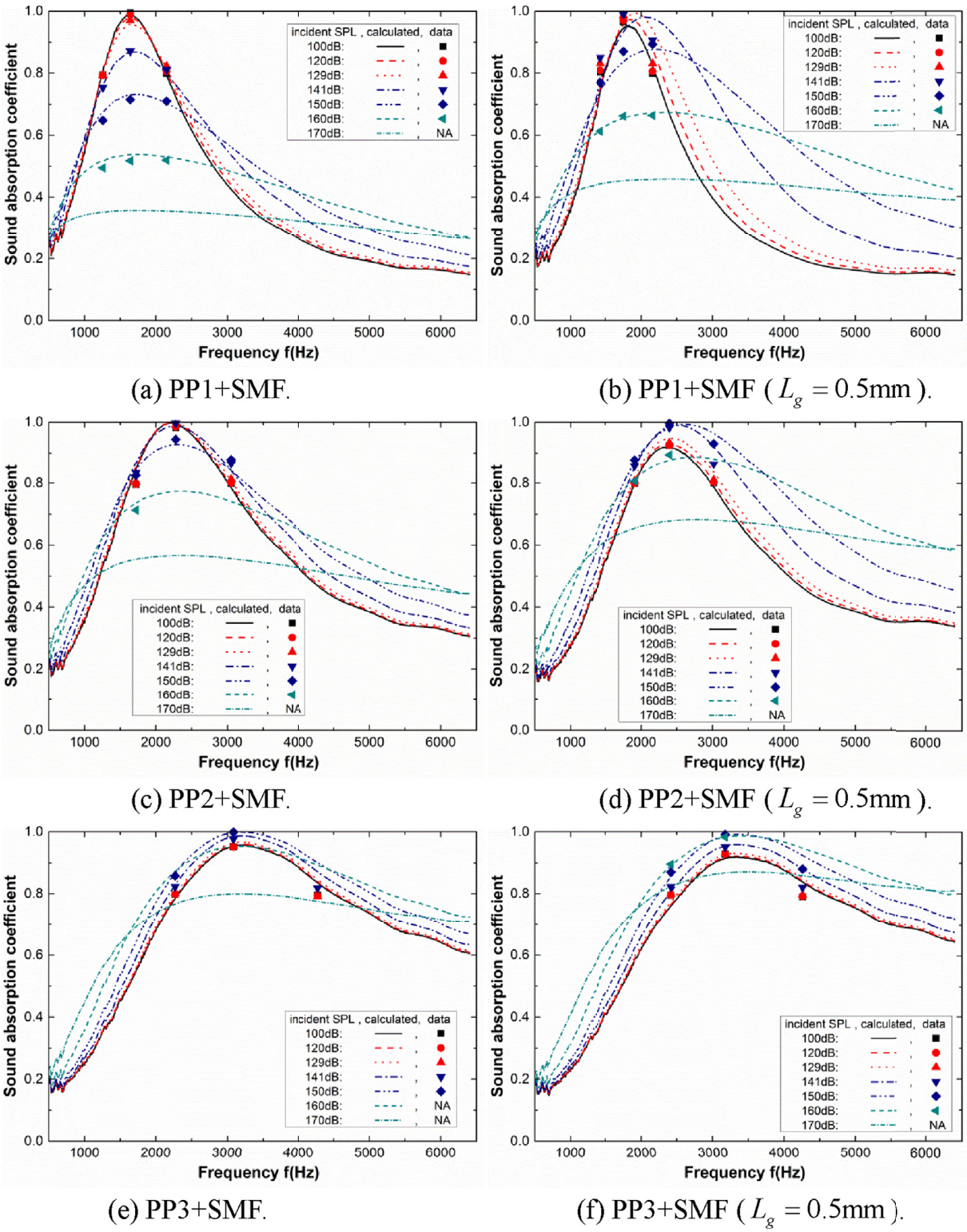

Fig. 12. Sound absorption coefficient against frequency for various incident SPLs for the acoustical units with hard wall backing. (Note: the marker "NA" in the legend represents that the corresponding data is not available.)

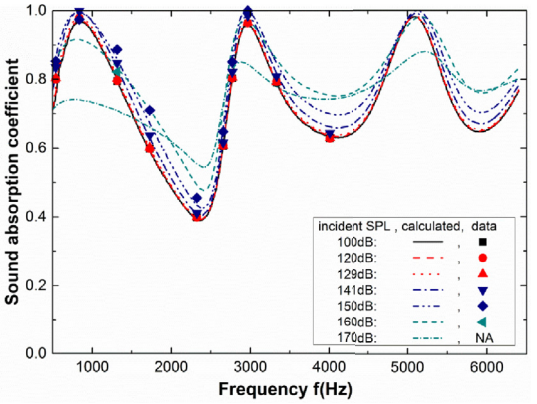

Fig. 13. Sound absorption coefficient against frequency for various incident SPLs for the acoustical unit PP3+SMF backed by an air cavity with 60 mm in depth. (Note: the marker "NA" in the legend represents that the corresponding data is not available.)

4. Conclusions

This paper proposes a model for predicting the sound absorptive performance of an acoustical unit in the form of a porous layer covered by a perforated panel under pure tones at high SPLs. Experiments are conducted to validate this model, and the experimental results, especially the measured acoustic resistance, agree well with the predicted results at different incident SPLs. The test results of the steady flow resistance show that the interference effect between the PP and the porous layer is correlated to the width of the air gap located between them. When the PP closely contacts with the porous layer, the interference effect induces significantly additional nonlinear flow resistance, which becomes larger with the decrease of perforation ratio of the PP. Correspondingly, the results of sound absorption of the acoustical unit at high SPLs show that the interference effect will alter the nonlinear acoustic impedance of the unit; therefore, such interference effect at high SPL should be considered in the design of this type of acoustical unit.

The theoretical and experimental results show that similar to the nonlinear absorptive properties of a single porous layer or a single PP, the sound absorptive performance of the acoustical unit also varies with the increase of incident SPL mainly in two trends: 1) the sound absorption coefficient will increase first and then decrease, corresponding to the under-resistance state under linear condition; 2) the sound absorption coefficient will monotonously decrease with the increase of SPL, corresponding to the over-resistance state under linear condition. The nonlinear coefficient of the porous material and the nonlinear parameter of the PP are the main factors determining the effective range of SPL with high sound absorption. For the design of this type of sound absorber, in order to achieve high sound absorption within a range of SPLs or at a specific SPL of the working condition in practical applications, two guidelines are suggested: 1) to design an acoustical unit whose absorption is relatively weakly dependent on the incident SPL, choose a porous layer with smaller Forchheimer's nonlinear coefficient and a PP with higher perforation ratio; 2) place the acoustical unit in the state of under-resistance under the linear condition by properly choosing the PP and the porous material, and design the critical SPL to be near the specific SPL of the working condition.

Acknowledgments

This work has been supported by the National Natural Science Foundation of China (Nos. 11404369 and 11574344), National Basic Research Program of China (No. 2012CB720203), and National Key Technologies Research & Development Program of China (No. 2016YFC0801704). The author gratefully appreciates some suggestions of Professor X.L. Wang and support from Professor J. Yang of the Institute of Acoustics. The author acknowledges H. Liang, Z.H. Huang and W.B. Wang of the Institute of Acoustics for their experimental assistance. The author thanks the Northwest Institute for Nonferrous Metal Research for providing sintered metallic fibers. The author would like to thank Professor Q. Min of Honghe University for his helpful suggestions in amending the paper.

References

[1] S.H. Park, A design method of micro-perforated panel absorber at high sound pressure environment in launcher fairings, J. Sound Vib. 332 (2013) 521–535.
[2] U. Ingard, S. Labate, Acoustic circulation effects and the nonlinear impedance of orifices, J. Acoust. Soc. Am. 22 (2) (1950) 211–218.
[3] T.H. Melling, The acoustic impedance of perforates at medium and high sound pressure levels, J. Sound Vib. 29 (1) (1973) 1–65.
[4] A. Cummings, Acoustic nonlinearities and power losses at orifices, AIAA J. 22 (6) (1986) 786–792.
[5] D.-Y. Maa, Microperforated panel at high sound intensity, Acta Acustica 21 (1) (1996) 10–14.
[6] X.D. Jing, X.F. Sun, Sound-excited flow and acoustic nonlinearity at an orifice, Phys. Fluids 14 (1) (2002) 268–276.
[7] A.S. Hersh, B.E. Walker, J.W. Celano, Helmholtz resonator impedance model, Part 1: Nonlinear behavior, AIAA J. 41 (5) (2003) 795–808.

[8] C.K.W. Tam, H. Ju, M.G. Jones, W.R. Watson, T.L. Parrott, A computational and experimental study of resonators in three dimensions, J. Sound Vib. 329 (2010) 5164–5193.
[9] Q. Zhang, D.J. Bodony, Numerical investigation and modelling of acoustically excited flow through a circular orifice backed by a hexagonal cavity, J. Fluid Mech. 693 (2012) 367–401.
[10] M.J.T. Smith, Aircraft Noise, Cambridge University Press, Cambridge, United Kingdom, 1989.
[11] W.E. Zorumski, T.L. Parrott, Nonlinear Acoustic Theory for Rigid Porous Materials, NASA TN-6196, 1971.
[12] D.A. Nelson, Interaction of Finite-amplitude Sound with Air-filled Porous Materials, NASA CR 174885, 1985.
[13] H.L. Kuntz, D.T. Blackstock, Attenuation of intense sinusoidal waves in air-saturated, bulk porous materials, J. Acoust. Soc. Am. 81 (6) (1987) 1723–1731.
[14] D.K. Wilson, J.D. McIntosh, R.F. Lambert, Forchheimer-type nonlinearities for high-intensity propagation of pure tones in air-saturated porous media, J. Acoust. Soc. Am. 84 (1) (1988) 350–359.
[15] J.D. McIntosh, R.F. Lambert, Nonlinear wave propagation through rigid porous materials. I: Nonlinear parameterization and numerical solutions, J. Acoust. Soc. Am. 88 (4) (1990) 1939–1949.
[16] R.F. Lambert, J.D. McIntosh, Nonlinear wave propagation through rigid porous materials. II: approximate analytical solutions, J. Acoust. Soc. Am. 88 (4) (1990) 1950–1955.
[17] Y. Aurégan, M. Pachebat, Measurement of the nonlinear behavior of acoustical rigid porous materials, Phys. Fluids 11 (6) (1999) 1342–1345.
[18] O. Umnova, K. Attenborough, E. Standley, A. Cummings, Behavior of rigid-porous layers at high levels of continuous acoustic excitation: theory and experiment, J. Acoust. Soc. Am. 114 (3) (2003) 1346–1356.
[19] O. Umnova, K. Attenborough, H.C. Shin, A. Cummings, Response of multiple rigid porous layers to high levels of continuous acoustic excitation, J. Acoust. Soc. Am. 116 (2) (2004) 703–712.
[20] F. Peng, X.L. Wang, Y. Sun, B.J. Chang, K. Liu, Investigation on the sound absorption characteristics of porous metal plates at high sound pressure levels, Acta Acustica 34 (3) (2009) 266–274.
[21] X.L. Wang, F. Peng, B.J. Chang, Sound absorption of porous metals at high sound pressure levels, J. Acoust. Soc. Am. 126 (2) (2009) EL55–61.
[22] B. Zhang, T.N. Chen, Y.Y. Zhao, W.Y. Zhang, J. Zhu, Numerical and analytical solutions for sound propagation and absorption in porous media at high sound pressure levels, J. Acoust. Soc. Am. 132 (3) (2012) 1436–1449.
[23] P.H. Forchheimer, Wasserbewegung durch Boden, Z. Ver. Dtsch. Ing 45 (1901) 1781–1788.
[24] R.H. Bolt, On the design of perforated facings for acoustic materials, J. Acoust. Soc. Am. 19 (5) (1947) 917–921.
[25] U. Ingard, R.H. Bolt, Absorption characteristics of acoustic material with perforated facings, J. Acoust. Soc. Am. 23 (5) (1951) 533–540.
[26] U. Ingard, Perforated facing and sound absorption, J. Acoust. Soc. Am. 26 (2) (1954) 151–154.
[27] W.A. Davern, Perforated facings backed with porous materials as sound absorbers-An experimental study, Appl. Acoust. 10 (1977) 85–112.
[28] K.P. Byrne, Calculation of the specific normal impedance of perforated facing-porous backing constructions, Appl. Acoust. 13 (1980) 43–55.
[29] F.P. Mechel, Helmholtz resonators with added porous absorbers, Acustica 80 (3) (1994) 268–279.
[30] R. Tayong, T. Dupont, P. Leclaire, Sound absorption of a micro-perforated plate backed by a porous material under high sound exictation: measurement and prediction, Int. J. Eng. Technol. 2 (4) (2013) 281–292.
[31] D.-Y. Maa, Theory and design of Micro-perforated panel sound-absorbing constructions, Sci. Sin. 18 (1) (1975) 55–71.
[32] L. Rayleigh, Theory of Sound II, Macmillan, London, 1929.
[33] U. Ingard, On the theory and design of acoustic resonators, J. Acoust. Soc. Am. 25 (6) (1953) 1037–1061.
[34] J.F. Allard, N. Atalla, Propagation of Sound in Porous Media: Modelling Sound Absorbing Materials, second ed., John Wiley & Sons Ltd., West Sussex, United Kingdom, 2009.
[35] N. Atalla, F. Sgard, Modeling of perforated plates and screens using rigid frame porous models, J. Sound Vib. 303 (2007) 195–208.
[36] H. Bodén, Y. Guo, H.B. Tözün, Experimental Investigation of Nonlinear Acoustic Properties for Perforates, AIAA Paper 2006-2404, 2006.
[37] G.J. Zhang, B.L. Liu, J.J. Xiong, X.D. Li, An investigation of the nonlinear characteristics of a perforated plate configuration under broadband noise excitation, in: Proceedings of Internoise, 2006.
[38] ASTM E2611-09, Standard Test Method for Measurement of Normal Incidence Sound Transmission of Acoustical Materials Based on the Transfer Matrix Method, ASTM International, Pennsylvania, United States, 2009.
[39] ISO 9053, Acoustics – Materials for Acoustical Applications – Determination of Airflow Resistance, International Organization for Standardization, Geneva, Swizerland, 1991.
[40] ISO 10534-2, Acoustics – Determination of Sound Absorption Coefficient and Impedance in Impedance Tubes – Part2: Transfer-function Method, International Organization for Standardization, Geneva, Swizerland, 1991.
[41] I.L. Vér, L.L. Beranek, Noise and Vibration Control Engineering: Principles and Applications, second ed., John Wiley & Sons Inc., Hoboken, New Jersey, 2005.